To cite this version :

Modeling of high-feed milling and surface quality applied to Inconel 718

Thomas Jacquet[a,*], Guillaume Fromentin[a], David Prat[a], Fabien Viprey[a]

[a]Arts et Métiers Institute of Technology, LaBoMaP, Université Bourgogne Franche-Comté, HESAM Université, F-71250 Cluny, France

* Corresponding author. *E-mail address:* thomas.jacquet@ensam.eu

Abstract

In modern manufacturing, machining remains a vital process for complex mechanical components. In particular, the aerospace industry extensively employs high-feed milling techniques to machine complex geometries from nickel-based superalloys. This study focuses on the analysis and modeling of high-feed milling for Inconel 718 in 2.5-axis machining. Its objective is to develop a generalized model of high-feed milling that enables the prediction of surface topography. The proposed model integrates crucial geometric parameters of the tool and its exact kinematic within the machine, along with tool and machine deflections caused by cutting forces. A key novelty of this research lies in its capability to determine surface topography and its quality based on a generalized model, representing significant progress in the field of high-feed milling. To validate the model, experimental efforts are measured to characterize the cutting forces and system deflections during machining. The developed approach demonstrates its ability to model surface topography and to predict surface roughness. It also highlights the influence of tool and machine deflection on surface quality. This research contributes to the advancement of the application of high-feed milling in aerospace manufacturing by enhancing machining capabilities and improving part quality.

Keywords: Surface topography; Surface roughness; High-feed milling

1. Introduction

In the production of machined parts, surface quality plays a crucial role. Therefore, modeling surface quality is essential. In numerous studies, phenomenological models are developed based on experimental analysis of surface quality, including empirical laws [3] or the use of artificial neural networks and genetic algorithm [13]. However, these techniques are limited to specific cutting conditions and cannot be generalized [2]. More generalized models are developed through analytical modeling approaches relying on the numerical determination of surface topography using algorithms such as Z-buffer [14, 15] or multi-dexels methods [17] and are then validated through experimental analysis of surface quality. These approaches mostly consider the geometry of the tool using finite element method. However, in certain machining domains such as micro-milling for the medical field where specific surface qualities are required, analytical geometrical models of the mills are developed, integrating specific geometric parameters such as the run-out of the milling cutter [18]. Moreover, cutting behaviors are considered in certain studies, such as the plowing effect of the tool and elastic spring-back [16, 11] or the mini-

mum uncut chip thickness effect [18]. The mechanical behavior of the tool or the machine is also considered in diverse studies, including the modeling of its stiffness [4] or its dynamic behavior [10, 5, 16]. However, such models require the prior modeling, of the cutting forces, which often relies on a mechanistic approach [6, 8]. In a high-feed milling context, some studies develop phenomenological models to predict surface quality, which are hardly generalizable to different tools or cutting conditions. A surface texture model for a two-edge cutting tool is developed by [12]. However, similarly to the phenomenological models, this model is hardly generalizable to different tool geometries. Furthermore, the Z-buffer algorithms used for numerical simulation of surface topography are computationally intensive and do not easily enable the calculation of surface topography across the entire machined surface. Nevertheless, some methods have been developed to limit the computing time using modern GPU architectures [1]. However, these methods remain complex to implement due to the necessity of parallelizing calculations. In this study, a new generalized method for modeling surface quality is developed, considering the precise description of the cutting edges of a high-feed milling cutter and the deflection of the tool and the machine under the cutting forces.

2. Geometrical model of the high-feed milling operation

2.1. Model of the high-feed milling tool

The IMX10C4FD10010C high-feed milling insert, manufactured by Mitsubishi Materials Corporation and used in this study, is a toric tool with four cutting teeth and has a nominal diameter D of 10 mm. Its maximum permissible depth of cut is represented as $a_{p_{max}} = 0.7$ mm. By utilizing a curvilinear abscissa parameterized as s, the Tool Envelope can be characterized within a polar tool frame $R_{t_{pol}} = (O_t, \vec{r}, \vec{t}, \vec{z})$, with reference to the nominal tool profile geometry illustrated in Fig. 1. The Tool Envelope, denoted as $\overrightarrow{TE}$, is described as follows:

$$\overrightarrow{TE}(s) = \left(R_g + r_n \sin\left(\frac{s}{R_g}\right)\right)\vec{r} + r_n\left(1 - \cos\left(\frac{s}{R_g}\right)\right)\vec{z} \quad (1)$$

Here, r_n represents the nose radius of the milling cutter, R_g represents the major radius of the toric envelope of the tool, and R_{lub} represents the radius of the center lubrication channel.
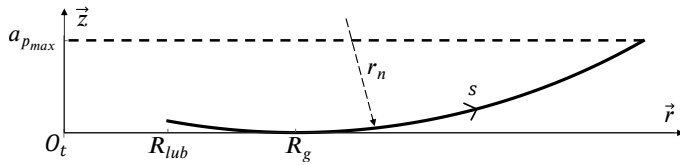

Fig. 1. Profile definition of the high-feed milling tool

Assuming that the rake faces are planar and identical for each tooth of the milling cutter, a reference rake face is represented using a reference Rake Plane $\overrightarrow{RP}_{ref}$ which is constructed using two unit vectors $\vec{u}$ and $\vec{v}$ within the tool frame $R_t = (O_t, \vec{x}, \vec{y}, \vec{z})$, alongside an arbitrary point M located within the rake plane. The reference Rake Plane is defined as:

$$\forall(a,b) \in \mathbb{R}^2, \; \overrightarrow{RP}_{ref}(a,b) = a\vec{u} + b\vec{v} + \overrightarrow{O_t M} \quad (2)$$

Utilizing local rake angle γ_n and edge obliquity angle λ_s, the reference rake plane is refined as:

$$\begin{aligned}\vec{u} &= \sin\gamma_n \vec{y} + \cos\gamma_n \vec{z} \\ \vec{v} &= \cos\lambda_s \vec{x} + \sin\lambda_s \vec{y}\end{aligned} \quad (3)$$

The rake faces of the tool are subsequently digitized using an optical 3D measurement system Alicona InfiniteFocusSL. Following this, the rake planes associated with the different teeth are determined using a mean squared error method in CATIA V5, which allows the identification of the γ_n and λ_s angles.

The reference Cutting Edge $\overrightarrow{CE}_{ref}$ can be defined as the intersection between the tool envelope and the reference rake plane. This intersection operation results in the identification of the change of variables $\psi : s \longmapsto (a,b)$, leading to the expression of the reference cutting edge as:

$$\overrightarrow{CE}_{ref}(s) = \left(\overrightarrow{RP}_{ref} \circ \psi\right)(s) \quad (4)$$

In physical terms, the reference cutting edge is limited to the center lubrication channel at $x = R_{lub}$ and the maximum permissible depth of cut at $z = a_{p_{max}}$, which can be expressed as a restriction on s such as $s \in [s_{min}, s_{max}] = \mathfrak{S}$ where:

$$\begin{aligned}\overrightarrow{CE}_{ref}(s_{min}).\vec{x} &= R_{lub} \\ \overrightarrow{CE}_{ref}(s_{max}).\vec{z} &= a_{p_{max}}\end{aligned} \quad (5)$$

Finally, each cutting edge, denoted as $\overrightarrow{CE}_{i_Z}$ and indexed by $i_Z \in [\![1, Z]\!]$, is defined in relation to the reference cutting edge in the following manner:

$$\overrightarrow{CE}_{i_Z}(s) = \overline{\overline{R}}_z(\alpha_{i_Z}).\left(\overrightarrow{CE}_{ref}(s) + \Delta x_{i_Z}\vec{x} + \Delta z_{i_Z}\vec{z}\right) \quad (6)$$

Here, $Z = 4$ is the number of teeth of the milling cutter, and α_{i_Z} denotes the relative angular position of the i_Z-th cutting edge with respect to the reference cutting edge, given by:

$$\alpha_{i_Z} = \frac{2\pi(i_Z - 1)}{Z} + \Delta\theta_{i_Z} \quad (7)$$

Additionally, $\Delta\theta_{i_Z}$, Δx_{i_Z} and Δz_{i_Z} represent the differential pitch, axial run-out, and the radial run-out of the i_Z-th cutting edge, respectively. Throughout this study, $\overline{\overline{R}}_k$ represents the direct rotation matrix around the k-axis. Experimental procedures were carried out to assess the axial and radial run-outs *in situ* employing a laser triangulation profilometer, but these measurements did not yield precise results. Consequently, in this study, the axial and radial run-outs are instead characterized using a tool presetter Nikken E46L. It is assumed that any run-outs introduced during the tool installation in the machine are negligible in this context. Additionally, the milling tool used in this study does not exhibit any differential pitch. However, it should be acknowledged that its inclusion in the cutting edge model could be a potential avenue for future research.

2.2. Surfacing operation model

In 3-axis milling, the trajectories of the cutting edges during machining are contingent on the rotation $-\theta$ of the milling cutter ($\theta \in \mathfrak{T}$ is defined positively in a counterclockwise direction) and the tool-path $\overrightarrow{\mathcal{T}}(\theta)$ of the tool center O_t. The geometrical Surface generated by the i_Z-th Cutting Edge during the machining movement $\overrightarrow{SCE}_{i_Z}$ which depict the trajectories of the cutting edges throughout the machining process, are defined as follows:

$$\overrightarrow{SCE}_{i_Z}(s, \theta) = \overrightarrow{\mathcal{T}}(\theta) + \overline{\overline{R}}_z(-\theta).\overrightarrow{CE}_{i_Z}(s) \quad (8)$$

The above definition can be applied to any 2.5-axis trajectory. However, for the purposes of this study, only a surfacing operation is considered, with a singular feed direction $-\vec{X}$ and successive i_p passes shifted in $\vec{Y}$ direction in the machine frame. Moreover, to facilitate the algorithmic approach, the surfaces generated by the cutting edges are distinctly separated for each pass i_p, as expressed below in the machine frame:

$$\begin{aligned}\overrightarrow{SCE}_{i_Z,i_p}(s,\theta) &= \overrightarrow{\mathcal{T}}_{i_p}(\theta) + \overline{\overline{R}}_z(-\theta).\overrightarrow{CE}_{i_Z}(s) \\ \text{with: } \overrightarrow{\mathcal{T}}_{i_p}(\theta) &= -Zf_z\frac{\theta}{2\pi}\vec{X} + a_e(i_p - 1)\vec{Y} - a_p\vec{Z}\end{aligned} \quad (9)$$

Here, a_e represents the radial depth of cut of the tool, a_p represents the axial depth of cut, and f_z represents the feed per tooth.

3. Machined surface model

3.1. Surface quality model

Formally, the height of the Machined Surface MS achieved in 2.5-axis milling can be defined at any point (x, y) on the workpiece as follows:

$$\text{MS}(x, y) = \min_{\forall(i_z, i_p)} \left(\overrightarrow{\widetilde{\text{SCE}}}_{i_z, i_p}(x, y) . \vec{Z} \right)$$

$$\text{where: } \overrightarrow{\widetilde{\text{SCE}}}_{i_z, i_p}(x, y) = \left(\overrightarrow{\text{SCE}}_{i_z, i_p} \circ \xi \right)(x, y) \tag{10}$$

In Eq. 10, $\xi : (x, y) \longmapsto (s, \theta)$ cannot be explicitly formulated due to the mathematically transcendental nature of the expressions describing the surfaces generated by the cutting edges. Consequently, the height of the machined surface also cannot be explicitly expressed. In this context, this height is discretely determined. An XY grid composed of points (x_i, y_j) is defined within the machine frame. The height of the machined surface is computed for each point on this XY grid using the method described below. The objective of this method is to avoid solving the implicit function ξ for each point on the XY grid by employing an interpolation method described below, which enables the computation of the height of the machined surface at that specific point. Initially, for each tooth and each pass, the surfaces generated by the cutting edges are segmented into localized portions $\overrightarrow{\text{SCE}}|_{\mathcal{P}_{i_z, i_p, K_s, K_\theta}}$ determined based on the subdivisions $\mathcal{P}_{i_z, i_p, K_s, K_\theta}$ of the $\mathfrak{S} \times \mathfrak{T}$ space where $(K_s, K_\theta) \in [\![1, N_s]\!] \times [\![1, N_\theta]\!]$, N_s representing the number of divisions along the cutting edge and N_θ representing the number of divisions within the angular rotation range (Fig. 2). Each portion has a curvilinear length of:

$$\Delta s = \frac{s_{max} - s_{min}}{N_s} \tag{11}$$

Additionally, each portion covers an angular range given by:

$$\Delta \theta = \frac{\theta_{max} - \theta_{min}}{N_\theta} \tag{12}$$

Here, θ_{max} and θ_{min} depend on the starting and ending points of the surfacing operation.

Then, points $P_{i_z, i_p, K_s, K_\theta, k_s, k_\theta}$, $(k_s, k_\theta) \in [\![1, n_s]\!] \times [\![1, n_\theta]\!]$ are calculated on each portion as follows:

$$P_{i_z, i_p, K_s, K_\theta, k_s, k_\theta} = \overrightarrow{\text{SCE}}|_{\mathcal{P}_{i_z, i_p, K_s, K_\theta}} (K_s \Delta s + k_s \text{d}s, K_\theta \Delta \theta + k_\theta \text{d}\theta) \tag{13}$$

Here, $\text{d}s = \frac{\Delta s}{n_s - 1}$ is the distance between the points $P_{i_z, i_p, K_s, K_\theta, k_s, k_\theta}$ along the cutting edge and $\text{d}\theta = \frac{\Delta \theta}{n_\theta - 1}$ the distance along the angular rotation range.

The points $P_{i_z, i_p, K_s, K_\theta, k_s, k_\theta}$ are then utilized to define an interpolating function $\overrightarrow{\widetilde{\text{SCE}}}_{i_z, i_p, K_s, K_\theta}$ on each portion, denoted as:

$$\overrightarrow{\widetilde{\text{SCE}}}_{i_z, i_p, K_s, K_\theta} : (x, y) \longmapsto \overrightarrow{\widetilde{\text{SCE}}}_{i_z, i_p, K_s, K_\theta}(x, y) \tag{14}$$

Those interpolating functions are piecewise linear and are constructed on a mesh of the XY space, employing T3 elements.

In accordance with its prior definition (Eq. 10), the height of the machined surface can be approximated by utilizing the interpolating functions as follows:

$$\text{MS}(x_i, y_j) = \min_{\forall(i_z, i_p)} \left(\min_{\substack{\forall(K_s, K_\theta) \\ (x_i, y_j) \in \mathcal{D}_{i_z, i_p, K_s, K_\theta}}} \overrightarrow{\widetilde{\text{SCE}}}_{i_z, i_p, K_s, K_\theta}(x_i, y_j) . \vec{Z} \right)$$
$$\tag{15}$$

where $\mathcal{D}_{i_z, i_p, K_s, K_\theta}$ represents the XY image domain of the corresponding surface of the cutting edge (Fig. 2).

Within this methodology, the interpolating functions serve to approximate the surfaces of the cutting edges. This approximation introduces a certain level of error in estimating the height of the machined surface. Nevertheless, the selection of appropriate values for $(\Delta s, \Delta \theta, \text{d}s, \text{d}\theta)$ allows to ensure that this error remains limited to a negligible magnitude of $0.1 \ \mu m$.
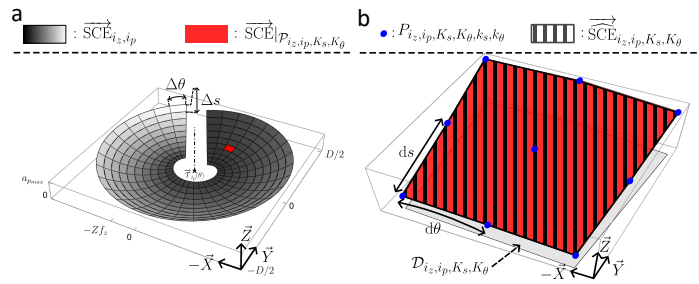

Fig. 2. (a) surface $\overrightarrow{\text{SCE}}_{i_z, i_p}$ of the i_Z-th cutting edge during one revolution of the mill for the i_p-th pass; (b) zoom on the interpolating function $\overrightarrow{\widetilde{\text{SCE}}}_{i_z, i_p, K_s, K_\theta}$ associated to the portion $\overrightarrow{\text{SCE}}|_{\mathcal{P}_{i_z, i_p, K_s, K_\theta}}$ of this surface.

Throughout the remainder of this study, the machined surface is computed for only a portion of the overall machined surface. This portion corresponds to the theoretical wavelengths of the machining process, which are Zf_z in the feed direction and a_e in the direction of successive passes. Reducing the surface in this manner allows for a more expedient computation of the surface topography and quality. However, this model reduction assumes that each pass is identical, with same tool angular position at the start. While this assumption may not hold true during actual machining, it is presumed that any differences between each pass are random in nature. Consequently, if the number of passes is sufficiently high, these random variations have an insignificant impact on the overall surface quality.

Nevertheless, it's important to note that in this study, the distinctions between passes are indeed considered. The topography and quality of the machined surface are examined at a local level, taking into account the variations between passes.

From the computation of the machined surface and in accordance with the norm *NF EN ISO 25178-2:2022*, surface quality can be described using various criteria including the arithmetic mean height S_a, the quadratic mean height S_q, and the maximum height S_z (in μm).

3.2. Run-out influence on the machined surface

Based on the machined surface model, numerical simulations have been carried out to assess the impact of the milling tool axial and radial run-outs on surface quality. Each of the simulations presented in Table 1 has been conducted with and

without run-outs (both axial and radial run-outs simultaneously), which have been previously determined.

For these numerical simulations, the XY grid points are spaced at intervals of 6 μm, and the effective diameter of the tool D_{eff} is approximately equal to 5.87 mm. Consequently, simulations No. 1 and No. 3 correspond to a cutting configuration where $2a_e < D_{eff}$, while simulations No. 2 and No. 4 correspond to a cutting configuration where $D_{eff} < 2a_e$.

Table 1. Numerical simulation parameters for evaluating the effect of run-outs on surface quality.

Simulation number	f_z (mm/tooth/rev)	a_p (mm)	a_e (mm)
No. 1	0.2	0.155	2
No. 2	0.2	0.155	5
No. 3	0.3	0.155	2
No. 4	0.3	0.155	5

In simulations No. 1 and No. 3, when run-outs are considered, the surface roughness criteria are approximately 5 to 6 times higher compared to the case where run-outs are disregarded. Moreover, the surface topographies exhibit significant differences in terms of both amplitude and wavelength (Fig. 3). Similar effects are observed in simulations No. 2 and No. 4, although these effects are relatively small in comparison to the predominant ridges left by the tool envelope between consecutive passes on the machined surface.

However, it's worth noting that in the context of semi-finishing or finishing operations where radial depth of cut is low, accounting for run-outs is crucial for accurately modeling surface quality and topography.

Furthermore, it is observed that the influence of radial run-out on the machined surface is negligible compared to the impact of axial run-out, primarily due to the significant difference in orders of magnitude between the X (or Y) dimensions in millimeters and the Z dimension in micrometers for the machined surface. As a result, for the remainder of this study, only the axial run-out and its predominant effect on the machined surface are considered.
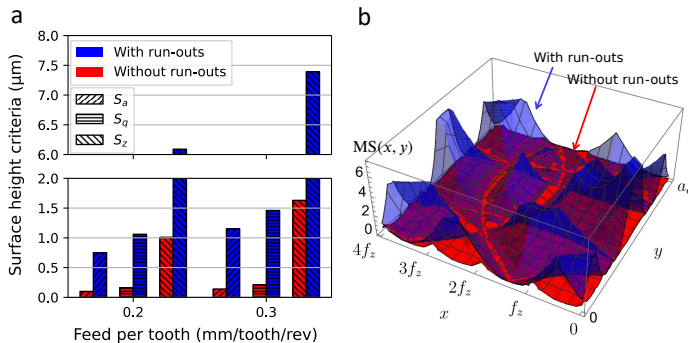

Fig. 3. (a) surface roughness criteria graph for numerical simulations No. 1 and No. 3; (b) machined surface topography (in μm) for simulation No. 3.

4. Modeling of the high-feed milling operation under cutting forces

4.1. Mechanical model of {tool, machine} system

The machined surface model that was previously developed considered only the geometry of the tool and the kinematics of the machining process. However, in this study, the effect of cutting forces on the machined surface, arising from the mechanical behavior of both the tool and the machine, is modeled. The deflection of the system {tool, machine} is parametrized by 2 degrees of freedom in translation along X and Y and 2 degrees of freedom in rotation around X and Y (Fig. 4). Tension-compression along Z is neglected due to the substantial rigidity of the Z axis compared to the X and Y axes. The stiffnesses associated with the 4 degrees of freedom are defined for an arbitrary point M in the machine frame as follows:

- The linear stiffness along $\left(M, \vec{I} \right)$:
$$k_{v_I}(M) = \frac{F_I(M)}{v_I(M)} \tag{16}$$

- The angular stiffness around $\left(M, \vec{I} \right)$:
$$k_{\alpha_I}(M) = \frac{F_I(M)}{\tan \alpha_I(M)} \tag{17}$$

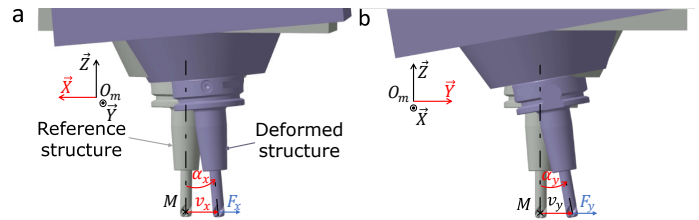Here, $F_I(M)$ represents the force applied to the system at point M, in I $\in$ [X, Y] direction.

Fig. 4. parametrization of the system deflection: (a) along $\left(M, \vec{X} \right)$; (b) along $\left(M, \vec{Y} \right)$

The linear and angular stiffness properties are determined through experimental characterization on a DMC65V 3-axes milling machine (Fig. 5). Likewise, for the X or Y axis of the machine, consecutive loading/unloading cycles are imposed on the system at point M and recorded using a Kistler 9257A dynamometer. This is achieved by moving the tool into contact with a highly deformable material (in this case, wood) through CNC-controlled motion. The linear displacements of the system relative to the machine frame are assessed at point M using triangulation with a laser displacement sensor Keyence LKG-32. Simultaneously, the X (or Y) axis of the CNC is measured to account for any deformation in the structure associated with the dynamometer. Subsequently, stiffness values are identified via linear regressions. In a similar manner, the angular rotations are characterized by measuring the local tangent of the system with a laser profile sensor (Keyence LJ-V7060) to obtain the local angular rotation around point M. In this experimental setup, point M is situated at the interface between the milling insert and its holder, where the tool geometry is cylindrical. This configuration is adopted to minimize the influence

of the tool rotation around its axis on the laser measurements when force is applied. However, it's important to mention that in this study, any differences in stiffness between point M and the tip of the milling insert are assumed to be negligible due to its relatively short length in comparison to the total length of the system along the Z axis. The average stiffness values identified from multiple cycles are summarized in Table 2, along with the 95% confidence interval identified during repeatability tests.
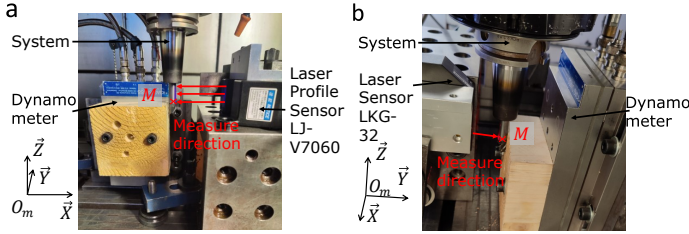
Fig. 5. experimental setup for the identification of system stiffnesses: (a) angular stiffness along Y; (b) linear stiffness along X

Table 2. Identified linear and angular stiffnesses of the system

Axis	Linear stiffness (N/μm)	Angular stiffness (10^5 N)
X	4.51 ± 0.31	2.8 ± 0.39
Y	7.88 ± 0.11	2.7 ± 0.83

4.2. Experimental characterization of the cutting forces

To model the deflection of the system, the cutting forces F_x and F_y exerted by the workpiece on the tool are characterized during up milling of an Inconel 718 workpiece during surfacing tests (Table 3). During these tests, the cutting forces along the X and Y axes are measured using a Kistler 9257A dynamometer, while the angular position θ of the tool is tracked using the incremental encoder of the machine spindle (Fig. 6a). The measurements of the cutting forces and the angular position of the tool are synchronized at a rate of 100 kHz. Then, following the approach by Ducroux et al. [9], the cutting forces are averaged at each identical tool angular position for every tool revolution during each pass of each test. Continuous functions $F_x(\theta)$ and $F_y(\theta)$ are then obtained through local linear interpolation of the measurements (Fig. 6b). For this characterization of the cutting forces, the torques on the system resulting from the eccentricity of the interface point between the Inconel 718 workpiece and the cutting edges (where the cutting forces are exerted from the workpiece to the tool) are not taken into consideration. Therefore, for the sake of model simplification, it is assumed that the cutting forces are applied to the tool at the intersection point between the tool axis and the tool envelope.

Table 3. Test plan parameters for the characterization of cutting forces and the evaluation of surface quality

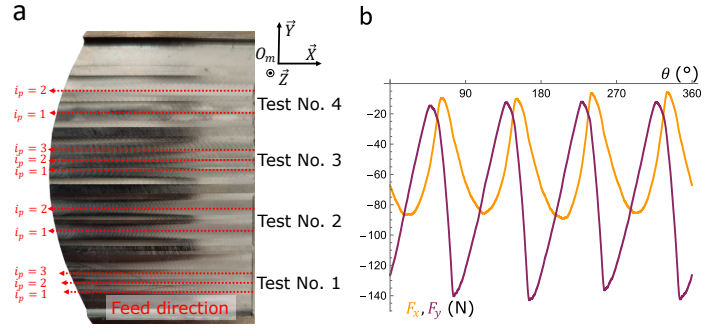| Test number	V_c (m/min)	f_z (mm/tooth/rev)	a_p (mm)	a_e (mm)
No. 1	25	0.2	0.155	2
No. 2	25	0.2	0.155	5
No. 3	25	0.3	0.155	2
No. 4	25	0.3	0.155	5

Fig. 6. (a) Inconel 718 test workpiece for the characterization of cutting forces; (b) experimental cutting forces obtained during the third pass of experiment No. 1. (mean forces over revolutions)

4.3. Mechanical model of the surfacing operation

The deflection of the system is incorporated into the surface quality model by redefining the Surfaces Generated by The Cutting Edges, where their trajectories are affected by the cutting forces. In accordance with Eq. 8, the deformed $\overrightarrow{\text{SCE}}_{\text{def}_{i_z,i_p}}$ are defined as follows:

$$\overrightarrow{\text{SCE}}_{\text{def}_{i_z,i_p}}(\theta) = \overline{\overline{R}}_{y_{\alpha_x}}.\overline{\overline{R}}_{x_{\alpha_y}}.\left(\overline{\overline{R}}_z(\delta\theta - \theta).\overrightarrow{\text{CE}}_{i_z}(s) - \overrightarrow{O_t M}\right)$$

$$+ \overrightarrow{O_t M} + \overrightarrow{\mathcal{T}}(\theta - \delta\theta) + \frac{F_x(\theta)}{k_x}\vec{X} + \frac{F_y(\theta)}{k_y}\vec{Y}$$

$$\text{where: } \overline{\overline{R}}_{y_{\alpha_x}} = \overline{\overline{R}}_y\left(\text{atan}\frac{F_x(\theta)}{k_{\alpha_x}}\right)$$

$$\text{and: } \overline{\overline{R}}_{x_{\alpha_y}} = -\overline{\overline{R}}_x\left(\text{atan}\frac{F_y(\theta)}{k_{\alpha_y}}\right) \tag{18}$$

Here, $\delta\theta$ represents the angular offset between the origin of the spindle incremental encoder and the first tooth of the mill cutter. This offset is experimentally determined for each test. The previously developed method for modeling the machined surface is then applied to these deformed surfaces of the cutting edges for each test, enabling the modeling of surface topography and quality while accounting for the deflection of the {tool, machine} system.

4.4. Assessment of the surface quality model

To evaluate the surface quality model, the machined surfaces obtained in each experimental test for cutting force characterization are digitized using an optical 3D measurement system Alicona InfiniteFocusSL and are compared with the model results, considering the same geometric conditions, and cutting forces. For simulations No.1 and No.3, the surface roughness criteria generally match between the model and the measurements (Fig.7a). However, differences in surface roughness criteria tend to increase as the feed increases. While most of the machined surface height aligns between the model and measurements, some ridges in the modeled surface are not present in the measurements (Fig.7b), this mismatch could be attributed to the oversight of the run-out evolution during machining. Additionally, the modeled surface topographies do not align with the measurements in terms of wavelength. This discrepancy can be

attributed to the absence of consideration for micro-geometrical defects in the model [7].

For simulations No. 2 and No. 4, similarly to the study on run-out effects on the machined surface, surface quality is primarily affected by the predominant ridge formed by the tool envelope between consecutive passes on the machined surface, despite the presence of similar phenomena observed in simulations No.1 and No.3. However, by simulating the model with and without angular or linear stiffnesses, it is numerically observed that the effect of the system linear stiffnesses on the machined surface is negligible in comparison to the effect of the angular ones due to the significant gap in orders of magnitude between the X (or Y) dimensions in millimeters and the Z dimension in micrometers for the machined surface. Furthermore, it is numerically observed that the effect of angular stiffness on the machined surface is of paramount importance when compared to the case where the deflection of the system is not considered.
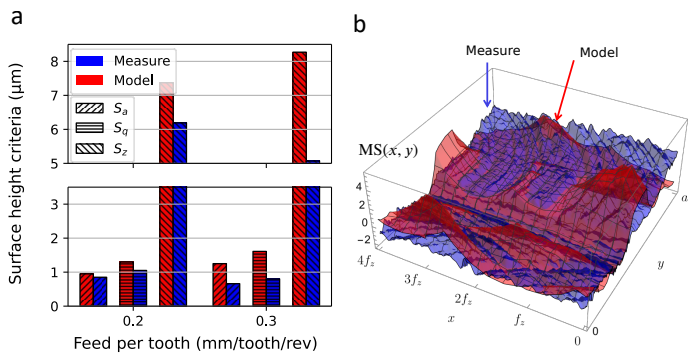

Fig. 7. (a) surface roughness criteria graph comparison between experimental data and the model; (b) machined surface topography (in μm) comparison between experiment No. 1 and the model

5. Conclusion and outlooks

This study introduces a comprehensive approach for modeling surface quality and topography, which is built upon a precise modeling of the milling tool cutting edges, including their run-out and tool and machine deflections caused by cutting forces. This characterization was experimentally conducted. Through this model, numerical simulations were employed to assess the significant influence of axial run-out and angular deflection of the tool and machine on the machined surface, and consequently, on surface quality. Furthermore, experimental tests on Inconel 718 provided a mixed validation of the model. Presently, the model relies on empirically measured cutting forces. To enhance predictability of surface quality, it may be advantageous to incorporate a mechanistic approach to model cutting forces. This could involve integrating tool wear effects into the cutting forces model [9] and considering its impact on the micro-geometry of the cutting edges. Moreover, tracking the run-out evolution during machining could provide valuable insight on surface quality. Integrating a mechanistic model of the cutting forces into the surface quality model would enable coupling between the mechanics and the geometry of the

process. However, adopting a mechanistic approach will necessitate the computation of uncut chip thickness, which cannot be approximated using standard methods due to specific high-feed characteristics [12]. The precise modeling of the cutting edges developed in this study could however provide valuable insights for the computation of uncut chip thickness.

References

[1] Abecassis, F., Lavernhe, S., Tournier, C., Boucard, P.A., 2015. Performance evaluation of cuda programming for 5-axis machining multi-scale simulation. Computers in Industry 71, 1–9.

[2] Abellan-Nebot, J., Bruscas, G., Serrano, J., Vila, C., 2017. Portability study of surface roughness models in milling. Procedia Manufacturing 13, 593–600. Manufacturing Engineering Society International Conference 2017, MESIC 2017, 28-30 June 2017, Vigo (Pontevedra), Spain.

[3] Alauddin, M., El Baradie, M., Hashmi, M., 1995. Computer-aided analysis of a surface-roughness model for end milling. Journal of Materials Processing Technology 55, 123–127.

[4] Araujo, A.C., Fromentin, G., 2018. Investigation of tool deflection during milling of thread in cr-co dental implant. The International Journal of Advanced Manufacturing Technology 99, 531–541.

[5] Arizmendi, M., Campa, F., Fernández, J., López de Lacalle, L., Gil, A., Bilbao, E., Veiga, F., Lamikiz, A., 2009. Model for surface topography prediction in peripheral milling considering tool vibration. CIRP Annals 58, 93–96.

[6] Armarego, E., Whitfield, R., 1985. Computer based modelling of popular machining operations for force and power prediction. CIRP Annals 34, 65–69.

[7] Biondani, F., Bissacco, G., 2019. Effect of cutting edge micro geometry on surface generation in ball end milling. CIRP Annals 68, 571–574.

[8] Budak, E., Altintas, Y., Armarego, E., 1996. Prediction of milling force coefficients from orthogonal cutting data .

[9] Ducroux, E., Fromentin, G., Viprey, F., Prat, D., D'Acunto, A., 2021. New mechanistic cutting force model for milling additive manufactured inconel 718 considering effects of tool wear evolution and actual tool geometry. Journal of Manufacturing Processes 64, 67–80.

[10] Elbestawi, M., Ismail, F., Yuen, K., 1994. Surface topography characterization in finish milling. International Journal of Machine Tools and Manufacture 34, 245–255.

[11] Feng, Y., Hung, T.P., Lu, Y.T., Lin, Y.F., Hsu, F.C., Lin, C.F., Lu, Y.C., Lu, X., Liang, S.Y., 2019. Surface roughness modeling in Laser-assisted End Milling of Inconel 718. Machining Science and Technology 23, 650–668.

[12] Huang, F., Jin, X., 2021. Surface texture generation using high-feed milling with spindle speed modulation. Precision Engineering 72, 13–24.

[13] Imani, L., Rahmani Henzaki, A., Hamzeloo, R., Davoodi, B., 2020. Modeling and optimizing of cutting force and surface roughness in milling process of Inconel 738 using hybrid ANN and GA. Proceedings of the Institution of Mechanical Engineers, Part B: Journal of Engineering Manufacture 234, 920–932.

[14] Jerard, R.B., Drysdale, R.L., Hauck, K.E., Schaudt, B., Magewick, J., 1989. Methods for detecting errors in numerically controlled machining of sculptured surfaces. IEEE Computer Graphics and Applications 9, 26–39.

[15] Lavernhe, S., Quinsat, Y., Tournier, C., Lartigue, C., Mayer, R., 2008. NC-simulation for the prediction of surface finish in 5-axis High-Speed Machining, in: 3rd CIRP International Conference on High Performance Cutting, Dublin, Ireland. pp. 387 – 396.

[16] Lu, X., Hu, X., Jia, Z., Liu, M., Gao, S., Qu, C., Liang, S.Y., 2018a. Model for the prediction of 3D surface topography and surface roughness in micro-milling Inconel 718. The International Journal of Advanced Manufacturing Technology 94, 2043–2056.

[17] Van Hook, T., 1986. Real-time shaded nc milling display. ACM SIGGRAPH Computer Graphics 20, 15–20.

[18] Yuan, Y., Jing, X., Ehmann, K.F., Zhang, D., 2018. Surface roughness modeling in micro end-milling. The International Journal of Advanced Manufacturing Technology 95, 1655–1664.